Journal of Analytical and Applied Pyrolysis xxx (xxxx) xxx–xxx

Contents lists available at ScienceDirect

Journal of Analytical and Applied Pyrolysis

journal homepage: www.elsevier.com/locate/jaap

Reactive carbons from Kraft lignin pyrolysis: Stabilization of peroxyl radicals at carbon/silica interface

Dhanalakshmi Vadivel[a,b], Andrea Speltini[a,*], Alberto Zeffiro[a], Vittorio Bellani[c], Sergio Pezzini[c,1], Armando Buttafava[a], Daniele Dondi[a,*]

[a] Department of Chemistry, University of Pavia, via Taramelli 12, 27100 Pavia, Italy
[b] Department of Chemistry, Bharathiar University, 641046 Coimbatore, India
[c] Department of Physics, University of Pavia, via Bassi 6, 27100 Pavia, Italy

ARTICLE INFO

Keywords:
EPR
Lignin
Pyrolysis
Pyrolytic carbon
Raman
Stabilized peroxide radicals

ABSTRACT

Lignin, the most abundant aromatic natural polymer and the second richest source of organic raw material, is considered as a potential source of energy, chemicals and carbon-based materials. In this work we have investigated the nature and reactivity of sp^2 carbons obtained by the pyrolysis of soluble Kraft lignin, a byproduct of paper making process. The formation of carbons from Kraft lignin deposited onto high surface area silica was studied by vacuum pyrolysis at different temperatures, using pristine and acid-washed lignin. Among the various techniques adopted for the material characterization, the Raman measurements showed that the procedure successfully yields carbon atoms organized in sp^2 domains, on the surface of silica, whose dimensions are submicrometric. The identification of a very stable peroxyl radical onto carbon-modified silica represents a major result, because these species are known to be usually transient. The observed peroxyl radicals are detectable only when both pyrolytic carbon and silica are present. The reactions of pyrolytic carbon onto silica with oxygen and nitrogen monoxide were studied by electron paramagnetic resonance (EPR). The kinetics and reversibility of the reaction with oxygen, as well as the reaction with nitrogen monoxide, were investigated.

1. Introduction

Carbon is the most important element for life on Earth due to the role it plays in organic chemistry because of the flexibility of its bonding, and carbon-based systems show an unlimited number of different structures with a variety of physical properties [1]. Even if it is one of the elements known from the ancient times, up to recent years new carbon materials have been discovered and extensively studied for various applications, viz. fullerenes, nanotubes, graphenes and graphitic carbon nitride [2,3]. As it is well known, in one of its allotropic forms carbon is the hardest of the known materials, and in another one it is among the softest. Diamond is transparent, electrically insulator and very hard, contrary to graphite, that shows a blackish colour and is an electrically conductive, soft material. The change of hybridization from sp^3 to sp^2 induces a modification of the crystallographic structure from cubic to hexagonal. Besides these pure allotropic forms, if both hybridization states are present or if there is a low amount of other elements (especially oxygen) or a variable amount of defects (in particular free radicals and dangling bonds), a huge variety of carbonaceous materials having properties in between can be produced.

Among the known carbonaceous solid materials, charcoal is the widest available and affordable. Charcoal is defined as the residue of solid non-agglomerated organic matter, of vegetable or animal origin, that results from thermal carbonization in the absence of air, at a temperature above 300 °C [4]. The physical properties of charcoal are unique, indeed the material can be a good (or poor) electrical conductor, it can show a high (or low) specific surface area, and it can have variable densities depending on the initial feedstock and the highest temperature employed in the carbonization procedure [5]. Charcoals and carbonized charcoals (biocarbons) and high-valued carbon nanomaterials can be prepared from a wide variety of biomasses [6,7]; the structure of such carbons depends not only on the temperature of preparation but also on the nature of the starting material. For these materials, surface area, particle size, porosity, inorganic content, as well as temperature and degree of carbonization, are all important parameters for classification [8].

On the other hand, vegetal biomass contains variable amounts of lignin (LG), a complex three-dimensional polymer composed of

* Corresponding authors.
E-mail address: andrea.speltini@unipv.it (A. Speltini).
[1] Present address: High Field Magnet Laboratory (HFML-EMFL) and Institute for Molecules and Materials, Radboud University, Nijmegen, 6525 ED, The Netherlands.

http://dx.doi.org/10.1016/j.jaap.2017.09.016
Received 17 January 2017; Received in revised form 28 July 2017; Accepted 18 September 2017
0165-2370/ © 2017 Elsevier B.V. All rights reserved.

phenylpropanoid units. It seems plausible that biocarbons derived from LG possess a graphite-like structure. Recent work reported that pyrolysis of lignocellulosic wastes is an easy, green route to prepare graphenes [9,10]. The LG base structure has in principle great potentiality to be rearranged in extended graphene-like aromatic layers, as demonstrated under microwave plasma irradiation [11] and also by pyrolytic treatment [12]. LG pyrolysis yields carbonaceous residues rich in polycyclic aromatic hydrocarbons [13,14], and polymeric carbon with fine sorption properties can be obtained from olive stones LG biomass [15]. It is also reported that softwood pyrolysis yields graphene sheets rearranged in turbostratic carbon [12]. LG can be considered as a waste material as it is the major by-product of second generation bioethanol production [16]. In particular, Kraft LG is obtained as a by-product of the paper pulping process. In the Kraft process the insoluble LG polymer present in wood is decomposed into smaller units under high temperatures (170–180 °C) in the presence of strong alkali solutions (sodium hydroxide) and sulfides. During the process the LG polymer backbone is broken and sulfides are included in the structure rendering it water soluble. The pyrolysis of LG, i.e. the treatment at high temperature in the absence of oxygen, leads to the elimination of sulfur and oxygen present in the polymer, thus leaving carbon as a residue. The LG backbone hydroxyphenylpropanoic units then can rearrange easily to give graphite-like extended aromatic structures. It is well known that the pyrolysis of Kraft LG proceeds in two steps according to the pyrolysis temperature. In the temperature range 200–400 °C carbon dioxide is produced together with volatile sulfur compounds [17], while in the range 500–600 °C carbon monoxide is evolved from phenols decomposition. Hydrogen gas production begins at 500 °C [18] indicating that, above this temperature, carbon defects are cured. The bulk pyrolysis of LG at high temperature (> about 3000 °C) is known to yield high-ordered carbon [19], and moreover supported carbons on inert inorganic materials can have very interesting properties and applications since they possess a conductivity by the sp^2 carbon sheets together with chemical reactivity and other relevant structural features; indeed inert supports (i.e. silica, hexagonal boron nitride, alumina and Si_3N_4) and pristine materials can be used for their preparation [20–24]. In this context, we showed that pyrolysis of Kraft LG deposited onto porous micrometric silica is an easy, effective route for silica surface modification with pyrolytic carbons [25]. A recent study described the free radicals in biochars from high temperature fast pyrolysis [26], but to the best of our knowledge the formation of radical species in the carbonaceous phase from pyrolysis of silica-supported LG has not been investigated.

In this work we deemed interesting and informative to study the nature and the reactivity of pyrolytic carbons generated on high surface area silica by using the vacuum pyrolysis technique. The pyrolytic carbons were extensively characterized by various techniques, that is Raman spectroscopy, electron paramagnetic resonance (EPR), thermogravimetric analysis (TGA) and attenuated total reflectance Fourier transform infrared spectroscopy (ATR-IR). The reactivity of the carbon phase was investigated by reaction with oxygen and nitrogen monoxide. Interestingly, stable peroxide radicals obtained by reaction with atmospheric oxygen were observed and thus further investigated.

2. Materials and methods

2.1. Precipitated silica zeosil 1165

Precipitated silica Zeosil 1165 was purchased from Rhodia (Bollate, Italy) and used as received. Zeosil 1165 possesses a four level fractal hierarchical structure consisting of primary particles of ca. 10 nm forming particle aggregates of ca. 300 nm giving in turn hard agglomerates; the latter structure ultimately forms soft agglomerates of 100–200 μm average size. Soft aggregates are disrupted by stirring in solvent dispersions. No evidence of a mesoporous structure is present. The total surface area, experimentally determined by nitrogen adsorption/desorption isotherms (B.E.T. method), was 160–165 $m^2\,g^{-1}$. The water content, determined by TGA considering the weight loss in the 100–130 °C range, was 3–4%. The dispersive and specific components of the surface energy, measured in a previous work [27] by inverse gas chromatography (IGC), are $\gamma_s^d = 96.0\ mJ\ m^{-2}$ and $I_{sp} = 142.6\ mJ\ m^{-2}$, respectively.

2.2. Kraft lignin

LG alkali low sulfur content was purchased from Sigma-Aldrich (Milan, Italy). The declared average molecular weight was 10,000 Da and the total sulfur content determined by elemental analysis is 2.89% (w/w). The product is soluble in water giving an alkaline solution. The amount of inorganic sulfate ion was determined to be 1.3% (w/w). The ash content at 600 °C was 17% with respect to dry LG. The amount of sulfate in ash was 44% (w/w). A titration with hydrochloric acid (37% w/w, Carlo Erba Reagents, Milan, Italy) performed by pH-meter measurements showed an equivalent point at 0.026 mmol H^+ for 100 mg LG. For further information about characterization see Ref. [17].

2.3. Acid-washed lignin

Acid-washed LG was prepared by adding dropwise concentrated hydrochloric acid (37% w/w) to a Kraft LG solution ($1\ g\ L^{-1}$) up to pH 1. The precipitate was collected after filtration through 0.45 μm Nylon filters. The residue was washed with a small amount of deionized water (the total yield of the process is 60% w/w). The ash content of acid-washed LG was 0.9% (w/w) with respect to the dry compound. The sulfate content of acid-washed LG was $30\ \mu g\ g^{-1}$ (0.003% w/w).

2.4. Pyrolysis experiments

For the preparation of carbon-derivatized silica, 50 mg of LG (Kraft or acid-washed) was dissolved in a proper solvent. In the case of Kraft LG, 50 mL of deionized water was used, whereas 150 mL methanol (HPLC gradient grade, VWR, Milan, Italy) was used for acid-washed LG, due to its low solubility in water. After the complete dissolution of LG, 1 g of Zeosil silica was added, the suspension was submitted to sonication for 30 min and the solvent was removed under vacuum. For the pyrolysis, 100–200 mg of sample were placed into an alumina combustion boat. The sample was placed inside a quartz tube inserted into a cylindrical oven (Watlow ceramic fiber heater, i.d. 38 mm, length 305 mm, electrical power 600 W). The vacuum (10^{-3} Pa) was obtained by a double stage diffusion and rotary vacuum pump. The heating rate of the oven was $600\ °C\ h^{-1}$ and the final temperature was kept for 20 min. Several pyrolysis temperatures (in the range 600–1200 °C) were explored in the above conditions. Each pyrolysis has been performed in triplicate to evaluate the reproducibility of the experiment. The reactivity of the pyrolytic carbons with atmospheric oxygen was as well investigated under ambient conditions after the pyrolysis of the material with the above reported procedure.

2.5. Study of the reactivity of the pyrolyzed material with nitrogen monoxide

The pyrolysis was performed by using the apparatus shown in Scheme 1 following the reported procedure with the exception that the sample (20 mg Kraft LG) was pyrolyzed directly inside an EPR quartz tube.

The sample was kept under dynamic vacuum until it reached ambient temperature, then the sample was kept under static vacuum by closing the valve on the sample. At this point, the three way valve was operated in order to connect the gas cylinder with the reservoir, that was filled with nitrogen monoxide. In order to better purify the gas, the reservoir was cooled with liquid nitrogen, then the vacuum valve was opened while keeping the nitrogen monoxide frozen. Subsequently,

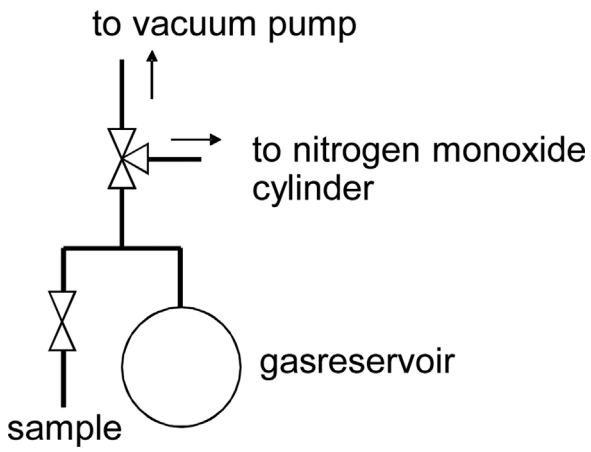

Scheme 1. Apparatus for the reaction with nitrogen monoxide.

under static vacuum conditions, the valve over the sample was opened to permit the contact with the gas and the liquid nitrogen was gently removed from the reservoir while keeping the reservoir temperature below −50 °C. This gas-cleaning procedure was used in order to remove eventual traces of NO_2 formed through the oxidation of NO in the presence of (possible) oxygen traces.

2.6. Raman spectroscopic measurements

Raman spectra were measured by a micro-Raman set-up (Horiba Jobin-Yvon Labram HR) with < 1 cm^{-1} spectral resolution, using a 100× objective (laser spot < 1 μm) and an excitation laser at 632.8 nm wavelength. The power on the samples was 6 mW.

2.7. Electron paramagnetic resonance measurements

The EPR instrument used for the measurements was a Bruker, EMX, X-band continuous wave spectrometer equipped with a EPR cavity Bruker ER4119HS. The measurements at different temperatures were made by using the Bruker kit for controlled temperature experiments.

2.8. Thermogravimetric analysis

The instrument used for TGA analysis was a Mettler Toledo TGA1 XP1. 8–10 mg of sample were inserted in an alumina crucible closed with a perforated lid. A blank performed with the empty crucible was subtracted from the curves. The heating rate was 10 °C min^{-1}, while the gas flow rate was 4 L h^{-1}. When nitrogen was used, a gas with low level (< 20 ppb) of oxygen was employed (gas cylinder with internal built-in purifier BIP filter from Sapio). For the analysis under nitrogen, the sample was purged with the gas at least for 30 min before starting the analysis. For the analysis under air, an oil-free membrane pump equipped with a pulsation damper and condensate drain was used.

2.9. Infrared spectroscopic measurement

ATR FT-IR measurements were performed using a Perkin Elmer 1600 FT-IR equipped with a Specac Mk II Golden Gate system. A total of 256 scans were recorded over 900–4000 cm^{-1} (resolution 2 cm^{-1}). The pressure applied on the sample was about 60 MPa.

3. Results and discussion

3.1. Pyrolytic carbon from kraft LG on zeosil silica

Fig. 1 shows the Raman spectra of four samples prepared at different temperatures (650 °C, 750 °C, 900 °C and 1100 °C). A subtraction of the

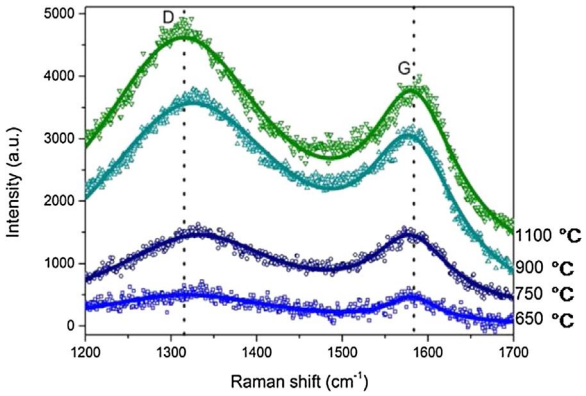

Fig. 1. Raman spectra of pyrolyzed Kraft LG@silica obtained under high vacuum after the subtraction of the background signal obtained from a reference pristine Zeosil silica (opens symbols; spectra from samples obtained at different temperatures are offset for clarity). Continuous lines are multi-Lorentzian fits to the G and D bands.

background signal collected on a reference Zeosil silica sample was performed to better evidence the effect of our treatment on the pristine silica.

The spectra clearly show a G band (1580 cm^{-1}) originating from the stretching mode of sp^2 C—C covalent bonds. An intense D band (1320 cm^{-1}) is also present, indicating a highly defective material. Both the G and D peaks become increasingly marked as the pyrolysis temperature increases, while their intensity ratio does not change significantly.

In particular, after thermal treatments the presence of defects in the carbon lattice is evidence by the increase of a D peak, due to intervalley resonant Raman scattering [28]. For a single carbon mono-layer, recent work have developed a method for quantifying the amount of disorder from the measurement of the ratio between the integrated intensity of the D and G peaks [28,29]. In this single carbon mono-layer approximation, the average distance between defective sites L_D is related to the ratio of the integrated intensity of the D and G peaks, I_D/I_G, which can be expressed as [28,29]:

$$\frac{I_D}{I_G} = C_A \frac{r_A^2 - r_S^2}{r_A^2 - 2r_S^2}\left[exp\left(-\frac{\pi r_S^2}{L_D^2}\right) - exp\left(-\frac{\pi (r_A^2 - r_S^2)}{L_D^2}\right)\right] + C_S\left[1 - exp\left(-\frac{\pi r_S^2}{L_D^2}\right)\right] \quad (1)$$

where $L_D = 1/\sqrt{s}$ is the distance between defects. Each defect is enclosed in a damaged region of radius r_s, around which there is an activated region, between r_S and r_A, which is the main reason for the increase of the D peak with disorder. In Ref. [28] the I_D/I_G changes are ascribed to the damages deriving from an intentional ion implantation. If we consider the damage deriving from other processes, for example the functionalization with diazonium salts, it gives a slightly different values of this ratio [30,31]. For this exemplificative case of damage from functionalization with diazonium salt, Wang and collaborators [30] used smaller values of r_S and r_A with respect to those used for implanted samples, because a covalent attachment site is less damaging for the lattice than an implanted ion. Thus in our calculations we employed the same values r_S = 0.07 nm and r_A = 1.0 of Ref. [30]. As regards the other two parameters, we used C_A = 4.97 and C_S = 0.94 which give ratios in agreement with the results of Table 1 of Ref. [29], which are close to the values employed in Ref. [28].

In Table S1 (Supplementary material) we report the values position w and line-width Γ of the G and 2D Raman peaks, the ratios of the integrated intensity I_D/I_G, the area concentration of defects s and the average distance between reacted sites L_D obtained from I_D/I_G using Eq. (1). Our Raman spectra reveal that increasing the temperature from 650 to 750, 900 up to 1100 °C, the I_D/I_G ratio increases monotonously from

Table 1
Number of spins per gram of carbon radicals determined by EPR in the samples pyrolyzed at two different temperatures.

Sample	Pyrolysis temperature (°C)	Number of spins/gram
Acid-washed LG@SiO_2	700	2.3×10^{19}
Acid-washed LG@SiO_2	900	4.3×10^{18}
Kraft LG@SiO_2	700	1.9×10^{19}
Kraft LG@SiO_2	900	1.3×10^{18}

2.6 to 3.2, due to the creation of sp^3 defects in the carbonic network, with a consequent reduction of L_D from 2.0 nm to 1.7 nm, in the approximation of applying the model of Eq. (1), developed for single carbon monolayer. These values are indicative, since they depend on the parameters used in Eq. (1).

The Raman analysis indicates that the method successfully yields C atoms arranged in sp^2 domains, immobilized on silica, whose dimensions are small as compared to the laser spot size (μm^2). FTIR spectra show the depletion of the $-OH$ group signal at 3400 cm^{-1} while increasing the pyrolytic temperature (spectra not shown). The peak is absent in the sample pyrolyzed at 1200 °C. Carbonyl stretching at 1620 cm^{-1} is visible in the non-pyrolyzed mixture of LG with silica but its intensity decreases accordingly with increasing pyrolytic temperature; in particular, in the sample produced at 1200 °C, the peak close to 1620 cm^{-1} is completely vanished. This clearly indicates that the presence of functional groups decreases by increasing the pyrolytic temperature, likely due the higher degree of condensation of the aromatic structures [9,25,26]; moreover, the C—H in-plane bending of the benzene ring decreases with increasing the pyrolysis temperature, which enhances the formation of sp^2 pyrolytic carbon, in good agreement with the Raman findings.

The carbon content after pyrolysis was measured by TGA, performed in air (the profiles are shown in Fig. S1, Supplementary material). This analysis revealed that neat Zeosil silica showed a weight loss of about 2% in the temperature range 200–1100 °C attributable to elimination of water from vicinal silanol groups. The silica with absorbed lignin before pyrolysis showed a total loss of 7%, while the samples pyrolyzed at 600 °C and 1200 °C showed weight losses of 5 and 4%, respectively. Moreover, the samples show a variable amount of absorbed water (10–20% w/w), released in the range 90–110 °C due to the hygroscopic properties of the silica used. The batch-to-batch reproducibility, evaluated on the TGA data, showed relative standard deviations (RSDs) below 0.5%.

The nature of the pyrolytic carbon onto Zeosil silica was assessed also by using EPR spectroscopy. The EPR spectra were measured at ambient temperature, showing a singlet signal clearly attributable to carbon centred radicals (g factor 2.0026), in agreement with recent work on fast pyrolysis of bulk lignocellulosic biomass [26]. Cr^{3+} was used as internal reference for the calculation of the 'g' factor. The neat Zeosil silica samples, either pristine or pyrolyzed in the same conditions with no adsorbed LG, did not give detectable EPR signals. After the final material was contacted with air, we detected new peaks (Fig. 2), due to two peroxyl radicals [27]. From the simulation of the spectra we obtained the following parameters: specie A: $g_1 = 2.045$, $g_2 = 2.0091$, $g_3 = 2.0024$ ($g_{iso} = 2.0188$, with the respective linewidths 7, 2 and 2 G); specie B: $g_1 = 2.0285$, $g_2 = 2.0102$, $g_3 = 2.0024$ ($g_{iso} = 2.0137$, with the respective linewidths 8, 4 and 2 G). The specie B fits particularly well with values reported for carbon or silicon peroxyl radicals [27], while specie A could be tentatively related to a SiOO radical close to alkaline centres. We never observed these radicals after pyrolysis of neither neat silica nor LG alone but their signals were detectable only when the precursor (mixture of both LG and silica) get pyrolyzed.

Surprisingly, the stability of the peroxyl radical was different from that reported in literature [27]. The kinetics of the growing radical was

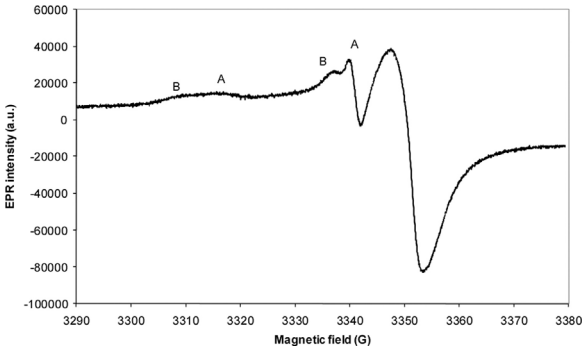

Fig. 2. EPR spectrum collected on Kraft LG@silica (pyrolyzed at 600 °C) after contact with air (oxygen reaction effect).

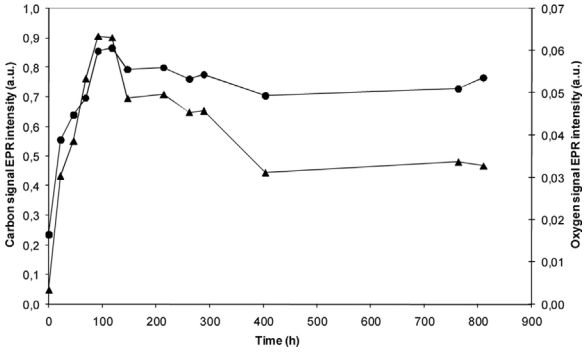

Fig. 3. Kinetics of the variation of carbon (triangles, left axis, measured at 3347 G) and peroxyl (circles, right axis, measured at 3337 G) radicals in pyrolytic carbon from Kraft LG@silica (pyrolyzed at 600 °C) after contact with air.

monitored for several days (see Fig. 3). During this period both the carbon peak and oxygen peak show a maximum of intensity close to 200 h after opening the vessel, while the subsequent plateau was kept for more than one month.

In order to better characterize the EPR signal, a saturation curve of the signal was studied as function of the applied microwave power. In fact, the saturation curve gives information about the relaxation time of the species. Lower is the relaxation time and lower is the saturability of the sample. Furthermore, if the spectrum is due to an overlap of different species having different saturation levels, this could be a method for a better characterization. For the carbon-centred signal, a very low saturation was observed up to 100 mW of applied microwave power (see Fig. 4), thus indicating the typical behaviour of highly conjugated carbon radicals, which possess good relaxation efficiency. The shape of the saturation curve might be typical of a non-homogeneously broadened resonance line [32,33].

In order to study the thermal stability of the radical we heated the

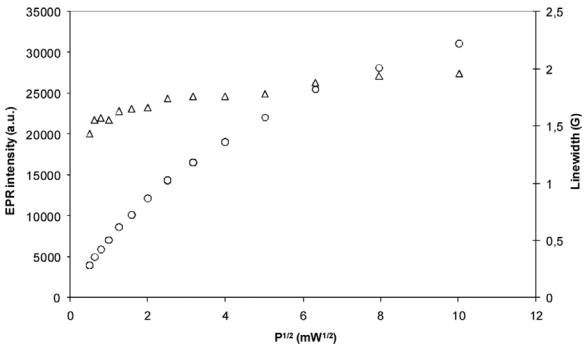

Fig. 4. Carbon saturation curves for Kraft LG@silica pyrolyzed at 900 °C (modulation amplitude: 0.2 G); circles: EPR intensity (peak height, left axis), triangles: peak linewidth (right axis).

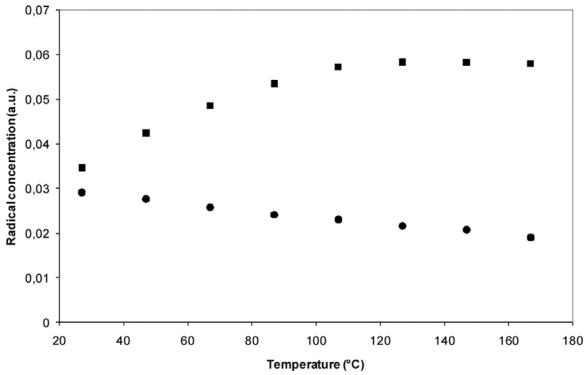

Fig. 5. Concentration of peroxyl radicals (squares, measured at 3337 G) and carbon radicals (circles, measured at 3347 G) determined by EPR in Kraft LG@silica as function of temperature.

sample up to 167 °C with temperature steps of 20 °C each, while the EPR spectra were recorded at ambient temperature, in order to permit a better comparison and to avoid decay during measurements. The relative peak heights of such experiments are plotted in Fig. 5. As it is apparent, a complete decay of peroxyl radicals is observed only at temperatures equal to or higher than 170 °C.

3.2. Pyrolytic carbon from acid-washed LG on zeosil silica

The Raman analysis, performed on samples produced from acid-washed LG at different temperatures, does not provide any evidence of graphitic carbon coverage, as the spectra were superimposable on the Zeosil silica reference background. This could be due to the absence of salts, especially alkalis that were proved to enhance the pyrolysis reaction [17]. Despite that, the EPR spectrum measured at ambient temperature, showed a peak clearly attributable to carbon centred radicals (g factor 2.0026). The saturation curve for this sample (Fig. 6) showed a good relaxation efficiency (low saturability). In fact, the EPR technique is a quite sensitive analysis by which low amount (< 1 ppm) of radicals can be detected and identified. Even for this sample, when the material was brought in contact with air, up to 800 h, new peaks around 3330 G and 3310 G appeared (Fig. 7). From the simulation of the spectra the following values $g_1 = 2.0133, g_2 = 2.0097$, $g_3 = 2.0024$ ($g_{iso} = 2.0133$, with the respective linewidths 8, 2 and 2 G) are associated to the peroxyl radical [27].

The kinetic of the reaction with atmospheric oxygen was measured for the acid-washed LG sample too (Fig. 8), observing a slow signal increase up to 300 h, after that the signal decreased. The behaviour was similar to that observed for Kraft LG.

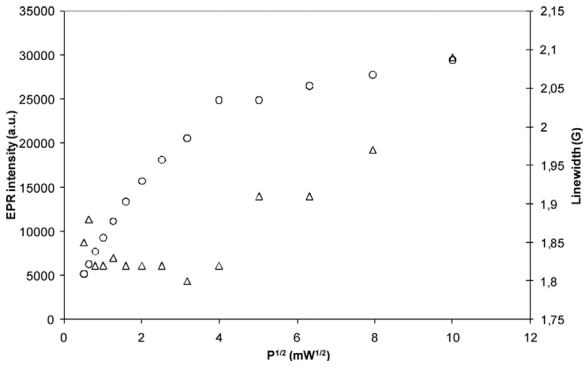

Fig. 6. Carbon saturation curves for acid-washed LG@silica pyrolyzed at 900 °C (modulation amplitude: 0.2 G); circles: EPR intensity (peak height, left axis), triangles: peak linewidth (right axis).

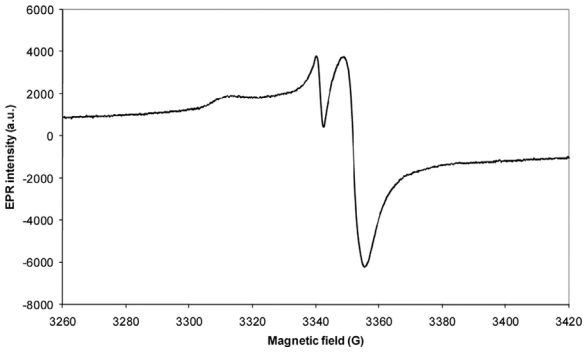

Fig. 7. EPR spectrum collected on acid-washed LG@silica (pyrolyzed at 600 °C) after contact with air (oxygen reaction effect).

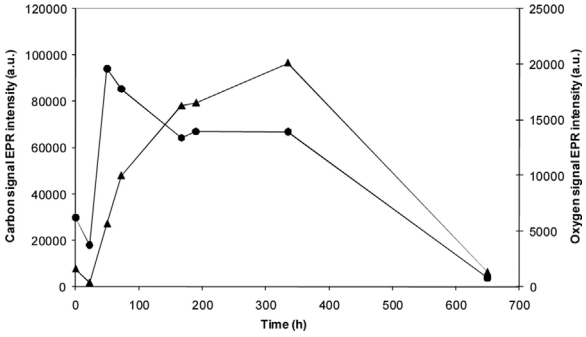

Fig. 8. Kinetics of the variation of carbon (triangles, left axis) and peroxyl radicals (circles, right axis) in pyrolytic carbon from acid-washed LG@silica after contact with air.

3.3. Spin radical concentration

Another method used to evaluate the quality of the carbon material formed, i.e. the number of defects leading to free radicals (like those on the zig-zag edges of the material), was the measure of EPR signal intensity, in fact the double integration of the EPR signal is proportional to the amount of radicals. Three independent calibration curves, signal area (y) vs. concentration of radicals (x), were plotted by using the stable radical 2,2,4,4-tetramethylpyperidinyloxide (TEMPO) as the standard compound. The concentration of radicals in the pyrolyzed samples, kept under high vacuum, was then expressed as number of spins per gram of material and is reported in Table 1. As expectable, while increasing the pyrolysis temperature the number of defects (i.e. spins) decreased. This confirmed that Kraft LG produces a better quality, less defective carbon material with respect to acid-washed LG, and this behaviour is more evident at the highest pyrolysis temperature, as the number of spin in acid-washed LG is three fold higher with respect to Kraft LG. This is in accordance with the high temperature enhancement of graphenic materials due to alkali and inorganic salts.

The formation of peroxyl radicals is an equilibrium reaction:

$$(C@SiO_2)\cdot + O_2 \rightleftarrows (C@SiO_2)\,O_2.$$

Indeed, oxygen can lead to some irreversible reactions (oxidation) on the substrate. The reversibility was demonstrated by putting the sample having peroxyl radicals under high vacuum at ambient temperature and measuring the amount of radicals by EPR at different times. After 6 h under vacuum the radicals reached a plateau, corresponding to a reversibility of about 70% (calculated with double integration of the EPR signal). The final radical species is compared with the starting material showing a slight decrease of linewidth (from 2.48 to 2.31 G, see spectrum in Fig. S2, Supplementary material).

3.4. Effect of nitrogen monoxide

The reactivity of carbon radicals was studied also putting in contact a gaseous radical compound with the pyrolyzed material in the absence of other atmospheric gases. In fact, because of the porous nature of the material, a gaseous radical seems be the best choice for studying the reactivity of carbon radicals, for instance nitrogen monoxide, as it can react with carbon radicals likewise the atmospheric oxygen.

$$(C@SiO_2)\cdot + NO\cdot \rightleftarrows (C@SiO_2)\,NO$$

This reaction is accomplished with a decrease in the total radical concentration of carbon. The reversibility of the reaction was studied after putting the sample under high vacuum (6 h at ambient temperature) and comparing the amount of radicals before and after the reaction. The reversibility of the reaction resulted to be of about 82%. The EPR spectrum acquired after the reaction showed an increase of the linewidth from 2.46 to 2.85 G (see spectrum in Fig. S3, Supplementary material). This effect could be related to a partial reaction of NO radicals over radical sites in pyrolytic carbon. Even the saturation was affected by the treatment; in fact, after the reaction the saturation occurs at higher power. This behaviour can be correlated to a selective irreversible reaction of the more reactive radicals (having less resonance and thus easier saturation) with respect to less reactive radicals.

4. Conclusions

Pyrolysis of lignin biomass onto silica for green preparation of supported reactive carbons was investigated. The Raman analysis revealed that lignin pyrolysis leads to production of carbon onto Zeosil silica with atoms arranged in sp^2 domains showing sub-micrometric size. The material, extensively characterized also by other physical-chemical techniques, showed the presence of exceedingly stable peroxyl radicals if contacted with air for several days. When Kraft (alkaline) lignin was used as the precursor, two different types of peroxyl radicals were evidenced by EPR spectroscopy. The effect of temperature on radicals at carbon/silica interfaces was also assessed, showing their stability up to 170 °C. The study of the reversibility of the reaction with oxygen indicated the presence of radicals having different reactivity (i.e. showing either reversible or irreversible reaction). The results here shown provide new insights in the pyrolysis products of Kraft lignin. The defective nature of the material obtained might be advantageous in view of a possible easy chemical functionalization, which mainly relies on the presence of radicals. In the future, we will explore the functionalization of such pyrolytic carbon materials, aiming at controlled tuning of their magnetic, optical and electronic properties.

Acknowledgements

We acknowledge the European Union for an ERASMUS MUNDUS Action 2 scholarship through the PANACEA project Agreement Number 2012-2647/001-001-EMA2 (European Commission) (D. Vadivel fellowship).

V.P and S.P. acknowledge the support by the Spanish Ministry of Economy and Competitiveness, under Projects MINECO/FEDER MAT2013-46308-C2-1-R and MAT2016-75955-C2-2-R.

Appendix A. Supplementary data

Supplementary data associated with this article can be found, in the online version, at http://dx.doi.org/10.1016/j.jaap.2017.09.016.

References

[1] A.H.C. Neto, F. Guinea, N.M.R. Peres, K.S. Novoselov, A.K. Geim, The electronic properties of graphene, Rev. Mod. Phys. 81 (2009) 109–162.
[2] A. Speltini, M. Sturini, F. Maraschi, A. Profumo, Recent trends in the application of the newest carbonaceous materials for magnetic solid-phase extraction of environmental pollutants, Trends Environ. Anal. Chem. 10 (2016) 11–23.
[3] Q.L. Yan, M. Gozin, F.Q. Zhao, A. Cohen, S.P. Pang, Highly energetic compositions based on functionalized carbon nanomaterials, Nanoscale 8 (2016) 4799–4851.
[4] W. Emrich, Handbook of Charcoal Making: The Traditional and Industrial Methods, Reidel D Publishing Company, Dordrecht, 1985.
[5] K. Mochidzuki, F. Soutric, K. Tadokoro, M.J. Antal, M. Toth, B. Zelei, G. Varhegyi, Electrical and physical properties of carbonized charcoals, Ind. Eng. Chem. Res. 42 (2003) 5140–5151.
[6] J. Bourke, M. Manley-Harris, C. Fushimi, K. Dowaki, T. Nunoura, M.J. Antal, Do all carbonized charcoals have the same chemical structure? 2. A Model of the chemical structure of carbonized charcoal, Ind. Eng. Chem. Res. 46 (2007) 5954–5967.
[7] J. Deng, Y. You, V. Sahajwalla, R.K. Joshi, Transforming waste into carbon-based nanomaterials, Carbon 96 (2016) 105–115.
[8] F. Rodriguez-Reinoso, Activated carbon: structure, characterization, preparation and applications, in: H. Marsh, E.A. Heintz, F. Rodriguez-Reinoso (Eds.), Introduction to Carbon Technologies, Universidad de Alicante, Alicante, 1997.
[9] L. Sun, C. Tian, M. Li, X. Meng, L. Wang, R. Wang, J. Yin, H. Fu, From coconut shell to porous graphene-like nanosheets for high power supercapacitors, J. Mater. Chem. A 1 (2013) 6462–6470.
[10] A. Suryawanshi, M. Biswal, D. Mhamane, R. Gokhale, S. Patil, D. Guin, S. Ogale, Large scale synthesis of graphene quantum dots (GQDs) from waste biomass and their use as an efficient and selective photoluminescence on-off-on probe for Ag^+ ions, Nanoscale 6 (2014) 11664–11670.
[11] Z. Wang, H. Ogata, S. Morimoto, J. Ortiz-Medina, M. Fujishige, K. Takeuchi, H. Muramatsu, T. Hayashi, M. Terrones, Y. Hashimoto, M. Endo, Nanocarbons from rice husk by microwave plasma irradiation: from graphene and carbon nanotubes to graphenated carbon nanotubes hybrids, Carbon 94 (2015) 479–484.
[12] O. Paris, C. Zollfrank, G.A. Zickler, Decomposition and carbonisation of wood biopolymers–a microstructural study of softwood pyrolysis, Carbon 43 (2005) 53–66.
[13] H. Zhou, C. Wu, J.A. Onwudili, A. Meng, Y. Zhang, P.T. Williams, Polycyclic aromatic hydrocarbon formation from the pyrolysis/gasification of lignin at different reaction conditions, Energy Fuel 28 (2014) 6371–6379.
[14] V.B.F. Custodis, C. Bährle, F. Vogel, J.A. van Bokhoven, Phenols and aromatics from fast pyrolysis of variously prepared lignins from hard- and softwoods, J. Anal. Appl. Pyrol. 115 (2015) 214–223.
[15] J. Simitzis, J. Sfyrakis, Pyrolysis of lignin biomass-novolac resin for the production of polymeric carbon adsorbents, J. Anal. Appl. Pyrolysis 26 (1993) 31–52.
[16] F. Cotana, G. Cavalaglio, A. Nicolini, M. Gelosia, V. Coccia, A. Petrozzi, L. Brinchi, Lignin as co-product of second generation bioethanol production from ligno-cellulosic biomass, Energy Procedia 45 (2014) 52–60.
[17] A. Dondi, A. Zeffiro, C. Speltini, D. Tomasi, A. Vadivel, the role of inorganic sulfur compounds in the pyrolysis of Kraft lignin, J. Anal. Appl. Pyrolysis 107 (2014) 53–58.
[18] S. Baumlin, F. Broust, F. Bazer-Bachi, T. Bourdeaux, O. Herbinet, F.T. Ndiaye, M. Ferrer, J. Lédé, Production of hydrogen by lignins fast pyrolysis, Int. J. Hydrogen Energ. 31 (2006) 2179–2192.
[19] J. Rodríguez-Mirasol, T. Cordero, J.J. Rodríguez, High-temperature carbons from Kraft lignin, Carbon 34 (1996) 43–52.
[20] E. Ruiz-Hitzky, M. Darder, F.M. Fernandes, E. Zatile, F.J. Palomares, P. Aranda, Supported graphene from natural resources: easy preparation and applications, Adv. Mater. 23 (2011) 5250–5255.
[21] T. Lin, Y. Wang, H. Bi, D. Wan, F. Huang, X. Xiec, M. Jiang, Hydrogen flame synthesis of few-layer graphene from a solid carbon source on hexagonal boron nitride, J. Mater. Chem. 22 (2012) 2859–2862.
[22] Z. Yan, Z. Peng, Z. Sun, J. Yao, Y. Zhu, Z. Liu, P.M. Ajayan, J.M. Tour, Growth of bilayer graphene on insulating substrates, ACS Nano 10 (2011) 8187–8192.
[23] Z. Tang, X. He, Y. Song, L. Liu, Q. Guo, J. Yang, Properties of mesoporous carbons prepared from different carbon precursors using nanosize silica as a template, New Carbon Mater. 25 (2010) 465–469.
[24] M. Sobiesiak, Thermal properties of nanoporous carbons prepared by a template method using different polymeric and organic precursors, New Carbon Mater. 27 (2012) 337–343.
[25] A. Speltini, M. Sturini, F. Maraschi, E. Mandelli, D. Vadivel, D. Dondi, A. Profumo, Preparation of silica-supported carbon by Kraft lignin pyrolysis, and its use in solid-phase extraction of fluoroquinolones from environmental waters, Microchim. Acta 183 (2016) 2241–2249.
[26] A. Trubetskaya, P. Arendt Jensen, A.D. Jensen, P. Glarborg, F. Hofmann Larsen, M. Larsen Andersen, Characterization of free radicals by electron spin resonance spectroscopy in biochars from pyrolysis at high heating rates and at high temperatures, Biomass Bioenerg. 94 (2016) 117–129.
[27] D. Dondi, A. Buttafava, A. Zeffiro, S. Bracco, P. Sozzani, A. Faucitano, Reaction mechanisms in irradiated, precipitated and mesoporous silica, J. Phys. Chem. A. 117 (2013) 3304–3318.

ARTICLE IN PRESS

[28] M.M. Lucchese, F. Stavale, E.H.M. Ferreira, C. Vilani, M.V.O. Moutinho, R.B. Capaz, C.A. Achete, A. Jorio, Quantifying ion-induced defects and Raman relaxation length in graphene, Carbon 48 (2010) 1592–1597.
[29] Q.H. Wang, Z. Jin, K.K. Kim, A.J. Hilmer, G.L.C. Paulus, C.J. Shih, M.H. Ham, J.D. Sanchez- Yamagishi, K. Watanabe, T. Taniguchi, J. Kong, P. Jarillo-Herrero, M.S. Strano, Understanding and controlling the substrate effect on graphene electron-transfer chemistry via reactivity imprint lithography, Nat. Chem. 4 (2012) 724–732.
[30] S. Niyogi, E. Bekyarova, M.E. Itkis, H. Zhang, K. Shepperd, J. Hicks, M. Sprinkle, C. Berger, C.N. Lau, W.A. de Heer, E.H. Conrad, R.C. Haddon, Spectroscopy of covalently functionalized graphene, Nano Lett. 10 (2010) 4061–4066.
[31] Z. Xia, F. Leonardi, M. Gobbi, Y. Liu, V. Bellani, A. Liscio, A. Kovtun, R. Li, X. Feng, E. Orgiu, P. Samorì, E. Treossi, V. Palermo, Electrochemical functionalization of graphene at the nanoscale with self-assembling diazonium salts, ACS Nano 10 (2016) 7125–7134.
[32] L.S. Singer, I.C. Lewis, D.M. Riffle, D.C. Doetschman, EPR characteristics of separated fractions of mesophase pitches, J. Phys. Chem. 91 (1987) 2408–2415.
[33] L. Khachatryan, J. Adounkpe, B. Dellinger, Radicals from the gas-phase pyrolysis of hydroquinone: 2. Identification of alkyl peroxy radicals, Energy Fuels 22 (2008) 3810–3813.